Circuit Properties and Device Characteristics of Printed Circuit Board Windings Employed as Contactless Energy Transfer Device

Jaehyun Nho, Wonseok Lim, Byungcho Choi, and Taeyoung Ahn*

School of Electronic and Electrical Engineering, Kyungpook National University, Taegu, Korea

* School of Electronics, Semiconductor, Computer/communication Engineering, Chongju University, Chongju-shi, Korea

ABSTRACT

Recent publications showed that a pair of neighboring printed circuit board (PCB) windings can be used as a contactless energy transfer device. As a continued study on this area, the current paper presents the modeling, analysis, and application of the neighboring PCB windings with an emphasis on their circuit properties and device characteristics as a contactless energy transfer device. Theoretical results of the paper are confirmed with experiments on a prototype contactless energy transfer circuit that delivers 24 W output power at 68 % efficiency through two 35 mm-diameter PCB windings separated each other by 2.4 mm.

I. INTRODUCTION

Earlier studies [1]-[3] have shown that a substantial inductive coupling exists between two spiral windings printed on the opposite sides of a double-sided printed circuit board (PCB). Accordingly, a doubled-sided PCB with spiral windings on its surfaces can be used as a substitute for the conventional core-based transformer for certain low-to-medium power applications, for examples, isolated gate drive circuits for MOSFETs/IGBTs [2] and low-profile dc-to-dc converters [3]. More recently, a contactless electrical energy transmission based on the inductive coupling between the neighboring PCB windings was investigated. In this study, two separate PCB windings, each built on a standard single-sided PCB, are placed closely in parallel as shown in Fig. 1(a). The feasibility of a contactless energy transfer using the PCB windings was reported in [4], and an adaptation of this concept to the battery charging circuits for portable electronics was presented in [5]. Fig. 1(b) shows the configuration of the contactless battery charger proposed in [5] for the applications to cellular phones. The desk-top unit, the primary side of the charger, contains the primary PCB winding together with associate electronics. The secondary side of the charger consists of the secondary PCB winding and the battery charging circuit along with a lithium-ion battery. An inductive coupling between two paralleled PCB windings, one on the top of the desk-top unit and the other on the bottom of the battery pack, provides a contactless energy transfer. One apparent merit of the proposed method is that the charging circuit does not noticeably increase the height, size and weight of the application system, thereby, making it adaptable to low-profile hand-held electronics.
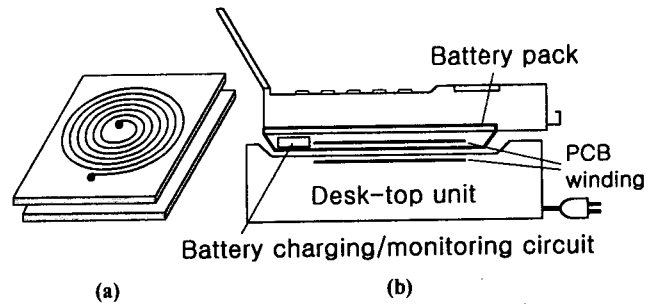

Fig. 1. Neighboring PCB windings and contactless charger for cellular phones. (a) Neighboring PCB windings. (b) Contactless charger for cellular phones.

As an extension of and supplement to the earlier publications [4]-[5], the current paper presents the modeling, analysis and application of the neighboring PCB windings focusing on their device characteristics as a contactless energy transfer device and their performance within the application circuit. This paper presents a circuit model for the PCB windings that allows the analysis and design of the application circuit to be performed using conventional circuit analysis techniques. Using the circuit model, this paper analyzes the circuit properties of the PCB windings and addresses their impacts on the design and implementation of the application circuit. This paper also presents the effects of the operating conditions on the device characteristics of the experimental PCB windings and performance of the prototype application circuit that transfers 24 W output power at 68 % efficiency through two spiral PCB windings separated each other by 2.4 mm.

II. CIRCUIT MODEL FOR PCB WINDINGS

This section presents a circuit model for the PCB windings. A pair of neighboring PCB windings are initially modeled as the magnetically coupled coils, and subsequently transformed into an equivalent circuit that does not involve magnetic coupling. The accuracy of the circuit model is verified by measurements on the experimental PCB windings.
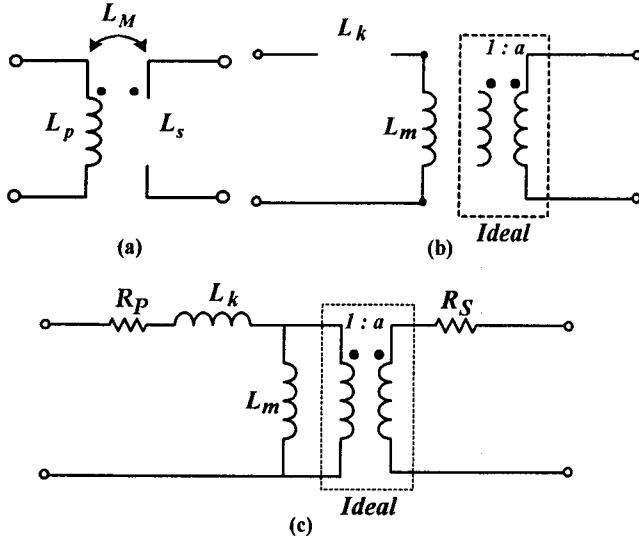
(a) (b) Ideal

(c) Ideal

Fig. 2. Circuit model for neighboring PCB windings. (a) Symbol of magnetically coupled coils. (b) Equivalent circuit model. (c) Circuit model with parasitic components.

A. Model Derivation

Fig. 2(a) show the circuit symbol for the magnetically coupled coils [6]. The neighboring PCB windings can be considered as the magnetically coupled coils whose inductive parameters are defined as:

● L_p : self inductance of the primary PCB winding

● L_s : self inductance of the secondary PCB winding

● L_M :mutual inductance of between the primary and secondary windings.

These parameters can be either analytically calculated [7] or experimentally measured. As regards the experimental evaluation of the parameters, the self inductance of each PCB winding can be individually measured and the mutual inductance can be found using the relationship

$$L_M = \frac{L_{add} - L_{opp}}{4}$$ (1)

where L_{add} is the inductance measured from two PCB windings connected in series in additive polarity and L_{opp} is the inductance of two PCB windings connected in opposite polarity. Once the inductive parameters are evaluated, Fig. 2(a) can be transformed into Fig. 2(b) keeping its terminal properties unchanged. The circuit parameters shown in Fig. 2(b) are given by [6]

$$L_k = L_p(1-k^2)$$ (2)

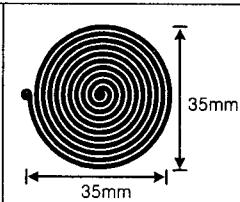$$L_m = k^2 L_p$$ (3)

$$a = \frac{L_s}{L_M}$$ (4)

where k is the coupling coefficient, defined as

$$k = \frac{L_M}{\sqrt{L_p L_s}}$$ (5)

Table I: Physical and electrical parameters of experimental PCB windings

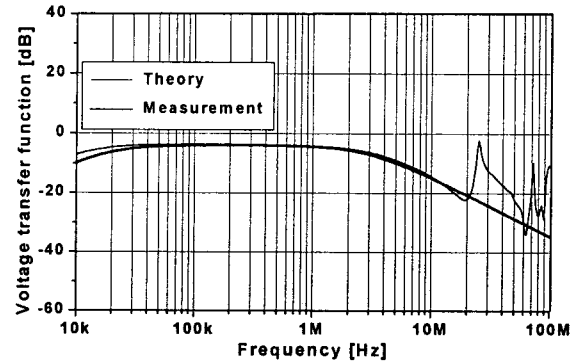| Physical parameters of PCB windings			
Primary winding		Thickness of cupper trace	90 μm
		Turns of trace	14
		Separation between traces	0.43 mm
		Width of trace	0.82 mm
Secondary winding	Same as the primary winding		
Electrical parameters of PCB windings with 2.4 mm separation			
$L_k = 1.46\mu H$, $L_m = 1.02\mu H$, $a = 1.57$ $R_p = R_s = 0.28\Omega$			

Fig. 3. Voltage transfer function of PCB windings loaded with 27Ω resistor.

The inductance L_k is referred to as the leakage inductance and L_m is called the magnetizing inductance, following the terminologies that have been used to quantity the non-ideal characteristics of conventional transformers. The dimensionless quantity a becomes the turns ratio of an ideal transformer used in the model. The parasitic components of the PCB windings can be incorporated into Fig. 2(b) resulting in the final model of Fig. 2(c). In Fig. 2(c), R_p and R_s represent the resistance of the primary and secondary windings. There exist parasitic capacitors within or between PCB windings, however, their capacitances are so small that they become influential only at very high frequencies, typically well above 10 MHz. Accordingly, if the operating frequency of the PCB windings is lower than 10 MHz, the parasitic capacitances can be ignored in the circuit model.

B. Model Validation

Table I shows the physical and electrical parameters of the experimental PCB windings that are used to show the accuracy of the proposed model. The PCB windings are fabricated on a standard single-sided PCB with 1 mm laminate thickness and 3 $ounce/ft^2$ cupper layer. The model parameters measured from the PCB windings separated each other by 2.4 mm (the laminate thickness of two PCBs plus 0.4 mm distance between PCBs) are listed in the lower part of Table I.
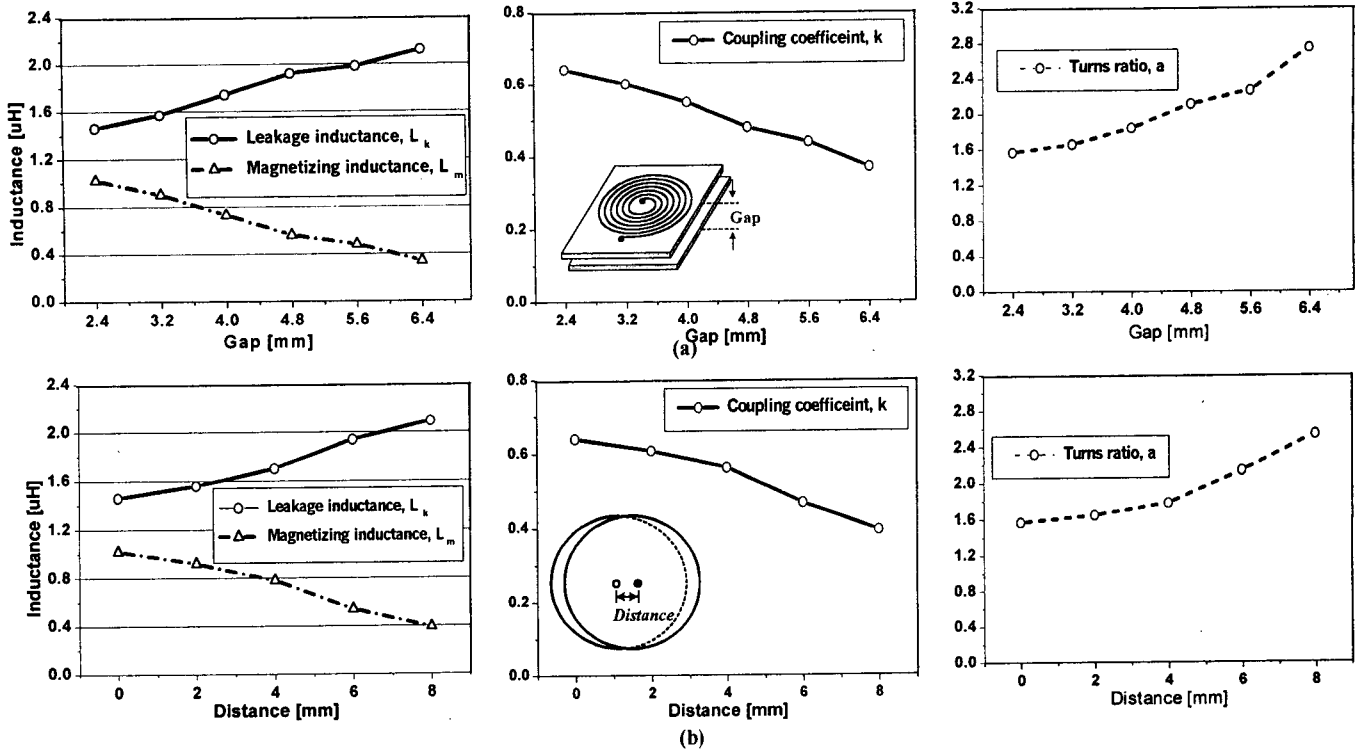
Fig. 4. Model parameters of PCB windings. (a) Parameter variation as gap changes. (b) Parameter variation as distance changes.

Interestingly, the leakage inductance, $L_k = 1.46 \mu H$, is larger than the magnetizing inductance, $L_m = 1.02 \mu H$, and the coupling coefficient is noticeably small, k = 0.64. All these, of course, are attributed to the existence of wide separation and absence of magnetic core between the PCB windings. The winding resistances, $R_p = R_s = 0.28 \Omega$, are also the important parameters since ohmic losses in the PCB windings could become very significant in certain applications.

Fig. 3 compares the input-to-output transfer function of the experimental PCB windings when a 27Ω load resistor is connected across the secondary winding. The thin line is the input-to-output voltage transfer function measured with HP4194A gain-phase analyzer. The thick line is the prediction of Fig. 2(c). Two curves show a close agreement up to 10 MHz and reveal deviations thereafter. The deviations at high frequencies are the effects of the parasitic components not accounted for in the model. Fig. 3 indicates that parasitic capacitances can be ignored when the operating frequency of the PCB windings falls below 10 MHz.

C. Model Parameters of Experimental PCB Windings

To study the device characteristics of the experimental PCB windings, their model parameters are evaluated while varying the operating condition. Fig. 4(a) is plots of the circuit parameters measured when the separation between PCB windings varied between $2.4 \, mm < gap < 4.8 \, mm$.
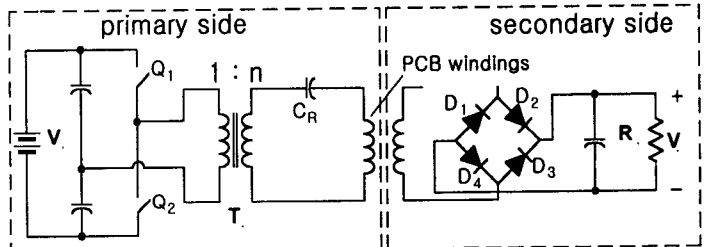

Fig. 5. Contactless energy transfer circuit : $V_S = 280V$, $C_R = 40nF$, $n = 0.1$, $R_L = 20\Omega$, $Q_1 - Q_2 : IRF840$, $D_1 - D_2 : 1N5819$, $D_3 - D_4 : URF4003$.

As the gap between PCB windings widens, the leakage inductance increases while the magnetizing inductance and coupling coefficient decrease. The turns ratio of the ideal transformer increases as the inductive coupling becomes weak, as can be predicted from (4).

Fig. 4(b) shows the circuit parameters when the separation is fixed at $gap = 2.4 \, mm$ but the cupper traces are off-centered due to the misalignment of the PCB windings. Fig. 4(b) shows the parameters when the distance between the cupper traces varied between $0 \, mm < distance < 8 \, mm$. The misalignment of PCB windings rapidly weakens the inductive coupling as the distance between the cupper traces increases.

III. PROTYPE ENERGY TRANSFER CIRCUIT

As an energy transfer device, the function of the coupled PCB windings is essentially identical to that of a
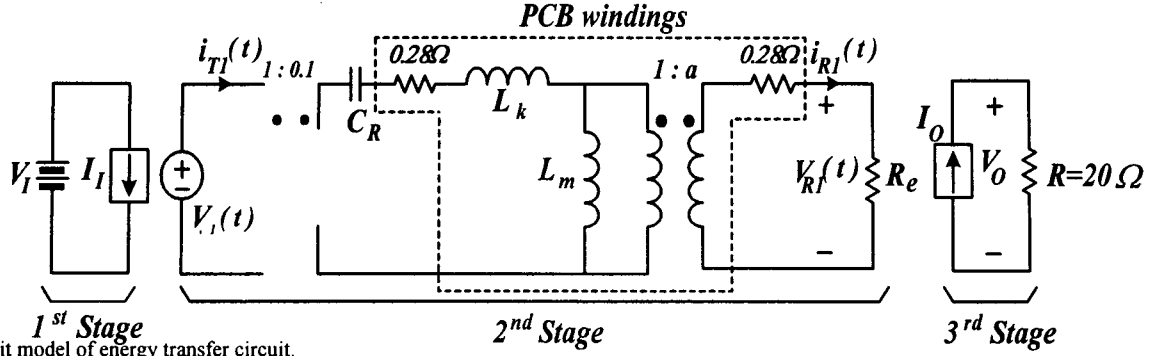
Fig. 6. Circuit model of energy transfer circuit.

conventional transformer. However, due to the presence of wide separation and absence of magnetic core, the leakage inductance of the PCB windings is considerably large compared with their small magnetizing inductance. A large leakage inductance could cause a substantial increase in the power loss, component stress, and switching noises to the application circuit. To resolve this problem, the application circuit can employ resonant or soft-switched converter topologies that absorb the leakage inductance as their circuit component. The resonant converter topologies are also advantages in that they minimize the harmonic components in the circuit waveforms, thereby easing the electromagnetic interference (EMI) problem that can be incurred by the PCB windings in operation. On the other hand, a small magnetizing inductance induces a large current to circulate within the application circuit. In turn, a large circulating current arouses significant conduction losses at the parasitic circuit components. In particular, ohmic losses at the PCB windings could become very large, often being a limiting factor to the power handing capacity of the application circuit. Accordingly, the methods to limit the circulating current to an acceptable level should be incorporated in the application circuit.

Fig. 5 shows a circuit diagram of the prototype energy transfer circuit that is designed to show application potentials of the PCB windings and to evaluate the performance of the experimental PCB windings. A half-bridge series resonant circuit is used on the primary side, that absorbs the leakage inductance of the PCB windings as an element of the resonant tank and allows a high frequency operation which is essential to reduce the circulating current. A conventional step-down transformer, T_R, is inserted between the switch network and the resonant tank to further reduce the circulating current. The secondary side of the experimental circuit consists of a high-frequency rectifier power by the secondary PCB winding, a filter capacitor, and a load resistor.

IV. PERFORMANCE OF ENERGY TRANSFER CIRCUIT

This section describes the voltage gain, efficiency, and output power of the prototype energy transfer circuit

Table II: Circuit variables and parameters for circuit model of energy transfer circuit

	Expressions
First stage	$V_I = \dfrac{V_S}{2}$, $I_I = \dfrac{2I_{TI}}{\pi}\cos\varphi_T$
Second stage	$v_{TI}(t) = \dfrac{4V_I}{\pi}\sin\omega_s t$ $i_{TI}(t) = I_{TI}\sin(\omega_s t - \varphi_T)$ $v_{RI}(t) = V_{RI}\sin(\omega_s t - \varphi_R)$ $i_{RI}(t) = I_{RI}\sin(\omega_s t - \varphi_R)$ $R_e = \dfrac{8}{\pi^2}R$
Third stage	$I_O = \dfrac{2}{\pi}I_{RI}$, $V_O = I_O R$

evaluated under various operating conditions.

A. Voltage Gain of Energy Transfer Circuit

Fig. 6 shows the circuit model for the energy transfer circuit obtained by adapting the circuit model of the PCB windings to the well-known modeling technique [10]-[11] for resonant converters. The model consists of three stages. The first stage is a dc model that represents the dc characteristics of the half-bridge switch network. The second stage is an ac model that describes the relationships between the fundamental components of the circuit waveforms. The second stage assumes that the higher-order harmonics of the circuit variables are well suppressed by the resonant tank and only the fundamental components are present in the circuit. The third stage models the dc characteristics of the load. The expressions for the circuit variables/parameters appearing in the circuit model are given in Table II.

From Fig. 6, the voltage gain of the energy transfer circuit can be recognized as

$$M = \frac{V_O}{V_S} = \left(\frac{V_I}{V_S}\right)\left(\frac{V_{TI}}{V_I}\right)\left(\frac{V_{RI}}{V_{TI}}\right)\left(\frac{I_{RI}}{V_{RI}}\right)\left(\frac{I_O}{I_{RI}}\right)\left(\frac{V_O}{I_O}\right) \quad (6)$$

Using the expressions given in Table II, the voltage gain can be evaluated as
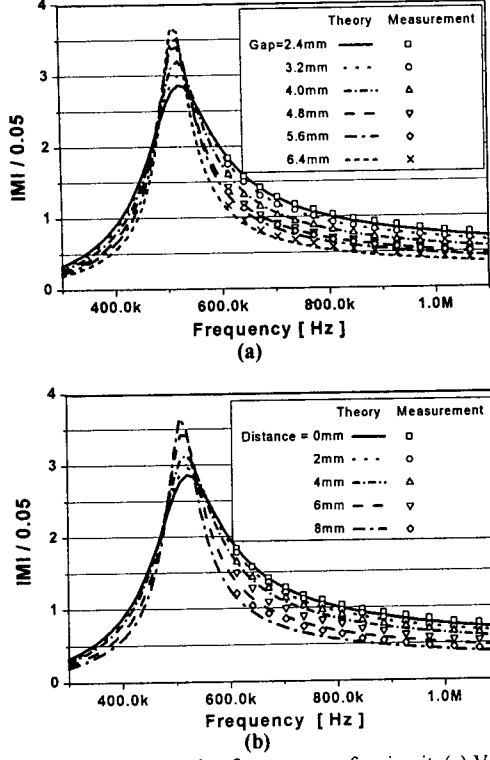
Fig. 7. Normalized voltage gain of energy transfer circuit. (a) Voltage gain with different gap. (b) Voltage gain with different distance.

$$M = 0.5 \frac{4}{\pi} H(s) \frac{\pi^2}{8R} \frac{2}{\pi} R = 0.5\, H(s) \qquad (7)$$

where $H(s)$ is the input-to-output transfer function of the second stage ac model. By evaluating $|H(s)|_{s=j\omega_s}$, the magnitude of voltage gain can be expressed as a function of the switching frequency, ω_s:

$$|M| = \frac{0.05}{\left[\left(\dfrac{L_k + L_m}{a L_m} - \dfrac{1}{\omega_s^2 a C_R L_m}\right) + j\left(\dfrac{a\omega_s L_k}{R_e} - \dfrac{a}{\omega_s C_R R_e}\right)\right]} \qquad (8)$$

The voltage gain of the circuit can now be analyzed by incorporating the circuit parameters of the PCB windings into (8). Fig. 7(a) shows the normalized voltage gain, $|M|/0.05$, of the energy transfer circuit when the separation between the PCB windings varied between $2.4\ mm < gap < 6.4\ mm$. Fig. 7(a) reveals that the voltage gain of the circuit closely resembles to that of a conventional series resonant converter. It is interesting to note that, as the separation increases, the voltage gain generally decreases but the damping factor of the circuit increases, thus boosting the gain in the neighborhood of the resonant frequency. Each theoretical curve is compared with experimental data. Since theoretical gain curves are valid only for frequencies above the resonant frequency of the tank circuit [10], the curves are experimentally verified at frequencies higher than 600 kHz. The experimental data show a good correlation with the analytical predictions, thereby validating the modeling and analysis method. Fig. 7(b) shows the voltage gain when the separation is fixed at $gap = 2.4\ mm$ but the
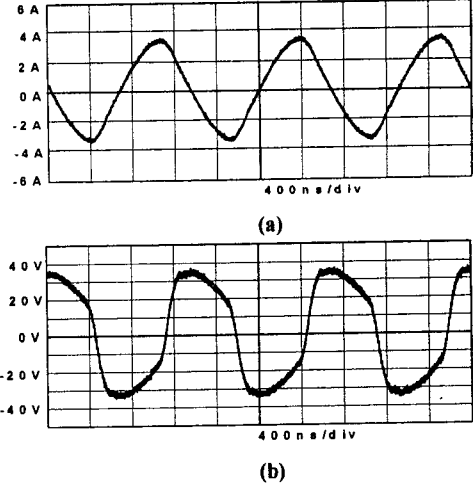

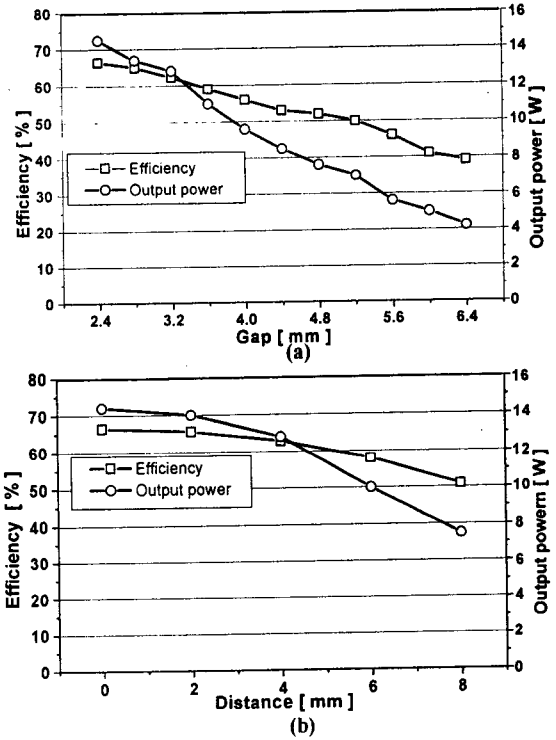Fig. 8. Current and voltage waveform of primary PCB winding. (a) Current. (b) Voltage.

Fig. 9. Efficiency and output power of circuit. (a) Measurements with different gap. (b) Measurements with different gap.

distance between the cupper traces varied as $0\ mm < distance < 8\ mm$. Similar to the previous case, the voltage gain decreases as the misalignment of the PCB windings extends. Fig. 7 indicates that the prototype circuit ensures a zero-voltage switching for all cases considered in this study, if the switching frequency, f_s, is selected higher than 530 kHz.

B. Circuit Waveforms, Efficiency, and Output Power

This section presents the performance of the prototype circuit operating with $f_s = 750\,kHz$, $V_S = 280V$, and $R_L = 20\,\Omega$.
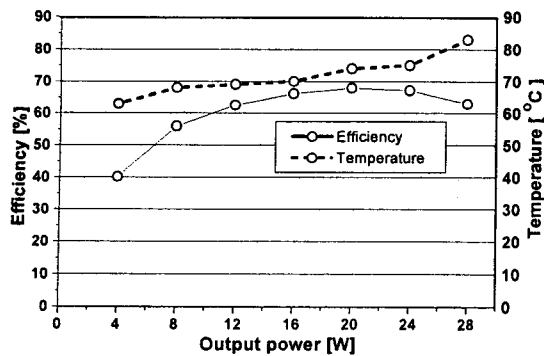
Fig. 10. Efficiency and PCB temperature with increased power levels.

Fig. 8 shows the current and voltage waveform of the primary PCB winding separated by 2.4 mm from the secondary winding. The current passing through the primary winding (Fig. 8(a)) is almost a sinusoidal wave. The voltage across the primary winding (Fig. 8(b)) is also smoothly filtered by inductances of PCB windings. These continuous and smooth waveforms alleviate the possible EMI problems associated with the PCB windings in operation.

Fig. 9(a) shows the efficiency and output power of the prototype circuit measured with different gaps between the PCB windings. A maximum efficiency of 66 % at an output power level of 14.5 W was measured with a 2.4 mm gap. As the gap increases, the efficiency and output power gradually decrease as the inductive coupling between the PCB windings becomes looser. With a 5.0 mm gap, the circuit delivers 7 W power at 50% efficiency. Fig. 9(b) shows the performance of the circuit with different distances between the cupper traces yet with a fixed gap at 2.4 mm. Similar to the previous case, both efficiency and output power decrease as the distance increases.

To evaluate the circuit performance at higher power levels, a series of experiments are performed using a current sink load. Fig. 10 shows the efficiency of the circuit and the surface temperature of the secondary PCB winding that operates with $f_S = 750\ kHz$, $V_S = 280V$, and $gap = 2.4$ mm. For the output power levels between 14 W to 24 W, an efficiency higher than 65 % is recorded with the PCB temperature lower than $75°C$. As the output power exceeds 24 W, the efficiency drops and the PCB temperature rises primarily due to the increase in ohmic losses at the PCB windings. The output voltage of the circuit is limited to a range of $16V < V_O < 18.6V$ for all experiments.

V. CONCLUSIONS

This paper presented the modeling, analysis and application of the neighboring PCB windings. The paper presented a circuit model that defines the PCB windings as a two-port network consisting of two inductive

parameters and an ideal transformer. As an application example, the paper introduced a half-bridge series resonant circuit that employs the PCB windings as an element of its tank circuit as well as a contactless energy transfer device. The analysis of this circuit demonstrated the use and accuracy of the proposed model for the PCB windings.

This paper also presented the performance of the prototype contactless energy transfer circuit focusing on the effects of operating conditions on the device properties of the PCB windings and performance of the application circuit. This study showed that a substantial inductive coupling exists at the presence of a considerable separation or misalignment between two opposing PCB windings. A prototype energy transfer circuit, implemented using two circular spiral PCB windings with 3.5 mm diameter, delivered 24 W output power through a 2.4 mm gap with an efficiency of 68%. Accordingly, it is envisaged that the PCB windings can be applied as an energy transfer device to the applications in which the PCB windings can be installed within close proximity of each other, such as a battery charger for hand-held electronics or a smart card for security systems.

REFERENCES

[1] S. Y. R. Hui, S. C. Tang, and H. Chung, "Coreless printed-circuit board transformers for signal and energy transfer," Electron. Lett., vol. 34, no. (11), pp. 1052-1054, 1998.

[2] S. Y. R. Hui, S. C. Tang, and H. Chung, "Optimal operation of coreless PCB transformer-isolated gate drive circuit with wide switching frequency range," IEEE Trans. Power Electron., vol. 14, pp. 506-514, May 1999.

[3] S. C. Tang, S. Y. R. Hui and H. Chung, "A low-profile low-power converter with coreless PCB isolation transformer," IEEE Trans. Power Electron., vol. 16, no. 3, pp. 311-315, May 2001.

[4] B. Choi, and J. Nho, "Contactless energy transfer using planer printed circuit board windings," Electron. Lett., vol. 37, no.(16), pp.1007-1009, 2001.

[5] B. Choi, J. Nho, and S. Choi, "A new contactless battery charger for portable telecommunication/computing electronics," will appear on Aug. 2001 issue of IEEE Trans. Consumer Electron.

[6] J. W. Nilsson, and S. A. Riedel, "Electronic circuits," Pretice Hall, New Jersey, 2001, 6th Ed. Appendix C, pp. 993-1001.

[7] W. G. Hurley, and M. C. Duffy, " Calculation of self and mutual inductances in planar magnetic structures, " IEEE Transactions on Magn.,, vol. 31, no. 4, pp. 2416-2422, July 1995.

[8] Y. Jang, M. Jovanovic, "A contactless electrical energy transmission system for portable-telephone battery chargers," IEEE INTELEC 2000 Record, pp.726-732.

[9] D. G. Pedder, A. D. Brown, J. A. Skinner, "A contactless electrical energy transmission system," IEEE Trans Ind. Electron., vol. 46, no. 1, pp. 23-30, Feb. 1999. .,"

[10] R. L. Steigerwald, " A comparison of half-bridge resonant converter topologies," IEEE Trans. Power Electron, vol. 3, no. 2, pp. 174-182, 1988.

[11] R. W. Erickson, and D. Maksimovic, "Fundamentals of power electronics," Kluwer, Norwell, MA. 2001, 2nd Ed. Chap. 19.